

A Model of the Effects of Hydrophone and Amplifier Frequency Response on Ultrasound Exposure Measurements

Gerald R. Harris, *Senior Member, IEEE*

Abstract—Because of finite amplitude effects in water or other low attenuation media, diagnostic ultrasound pressure pulses can have significant spectral content beyond 50 MHz. To record these pulses accurately, the hydrophone and its preamplifier must have a sufficiently broadband response. To examine how less-than-ideal hydrophones and amplifiers could affect the measurement of pulse parameters, a simulated distorted pressure pulse was analyzed before and after being filtered by hydrophone and amplifier response models. The hydrophone model used is similar to the response of piezopolymer membrane hydrophones. The amplifier model was taken from typical responses of integrated circuit operational amplifier-based designs. The pressure pulse, hydrophone, and amplifier were characterized respectively by the pulse center frequency, f_c , the hydrophone resonance frequency, f_h , and the amplifier low-pass corner frequency, f_a . It was found that if errors in the pulse-average intensity were to be below about $\pm 5\%$, then f_h/f_c should be greater than about 10 for the hydrophone alone, or f_a/f_c should be greater than about 8 for the amplifier alone. However, when considering both filter functions, a hydrophone-amplifier combination can be chosen to allow less restrictive frequency ratios because of the offsetting nature of the two filtering processes.

I. INTRODUCTION

MINIATURE ULTRASONIC HYDROPHONES having polyvinylidene fluoride (PVDF) sensitive elements are the devices of choice for making measurements in high amplitude ultrasound fields [1], [2]. Part of the reason lies in the potentially broadband response of these hydrophones. However, in practical hydrophone designs the thickness resonance frequency may occur within the band of frequencies comprising the ultrasonic pulse being measured. Furthermore, some hydrophone amplifiers may not have adequate bandwidth to reproduce faithfully all pulsed waveforms, especially those of high center frequency and large amplitude.

To study the errors that might result from using non-ideal hydrophones and amplifiers, a model was developed to simulate a pressure pulse before and after hydrophone detection and amplification. The errors introduced by these two components were computed by comparing var-

ious pressure and intensity (pressure squared) parameters for the original and processed waveforms.

The models for the pressure pulse, hydrophone, and amplifier are described in Section II. The simulation results are presented in Section III, and in Section IV recommendations are given for selecting the hydrophone resonance and amplifier corner frequencies relative to the center frequency of the pressure pulse.

II. PRESSURE PULSE, HYDROPHONE, AND AMPLIFIER RESPONSE MODELS

A. Pressure Pulse

Fig. 1 shows the temporal pressure pulse $p_i(t)$ used in these simulations. The mathematical model given in (1) was taken from Ayme and Carstensen [3].

$$p_i(t) = \left[\sum_{n=1}^{100} \frac{\sin(2\pi n f_c t + \pi/4)}{n} \right] \exp[-Q^2(t - t_1)^2]. \quad (1)$$

Here $p_i(t)$ is the summation of 100 n -weighted, phase-shifted harmonics with fundamental (center) frequency f_c , multiplied by a Gaussian envelope function; Q and t_1 control respectively the envelope width and time shift with respect to the summed sinusoids. Note that the fundamental pressure amplitude term P_F in [3] is omitted in (1) because it would cancel in the present analysis. In Fig. 1 $p_i(t)$ is plotted versus the scaled time $f_c t$, which was varied from 0 to 6, 6 being the number of cycles of the fundamental over which $p_i(t)$ was computed.

One hundred terms were summed to give a pulse representative of one likely to be encountered in practice; i.e., one that contains the compressional peaking, rarefactional rounding, and shock front formation associated with nonlinear ultrasound fields.

Four quantities were computed on this pulse before and after filtering: peak compressional (positive) pressure, p_c , peak rarefactional (negative) pressure, p_r , pulse pressure-squared integral, $p^2 I$ (indicative of the temporal average intensity), and pulse average intensity, I_{PA} [4].

B. Hydrophone Response Model

The hydrophone response function was derived from Mason's model for a piezoelectric transducer [5]. The

Manuscript received November 27, 1990; revised March 4, 1991; and accepted March 5, 1991.

The author is with the Food and Drug Administration, Center for Devices and Radiological Health, 5600 Fishers Lane, HFZ-132, Rockville, MD 20857.

IEEE Log Number 9101149.

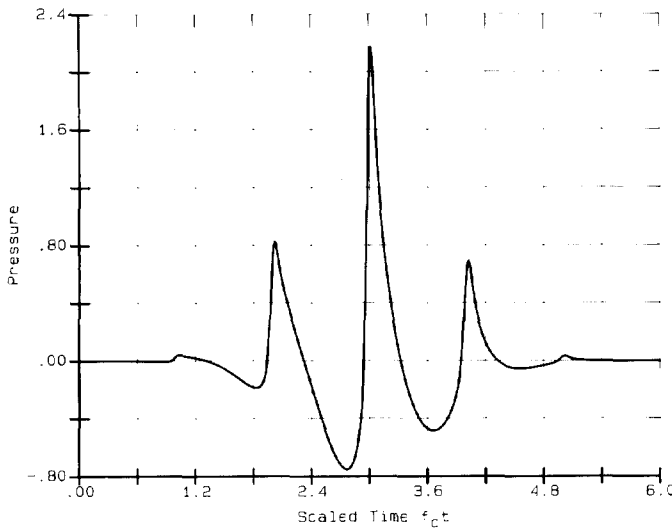


Fig. 1. Temporal pressure pulse $p_i(t)$ vs scaled time $f_c t$.

normalized response function $H_h(f)$ for the case of a symmetrically loaded receiver can be written as,

$$H_h(f) = \{\theta[\cot \theta + j(z_w/z_o)]\}^{-1} \quad (2)$$

where f is frequency, $j = (-1)^{1/2}$, z_w and z_o are respectively the acoustic impedances of water and PVDF, and $\theta = kd/2$, k being the wave number and d the PVDF thickness. Acoustic losses can be accounted for via a complex wave number, $k = 2\pi f/c - j\beta f$, where c and β are the sound speed and attenuation coefficient for PVDF.

A frequency scaling term $h = f_h/f_c$ was used, where f_h is the hydrophone thickness resonance frequency. For half-wave resonance, $f_h = c/2d$, so θ can be written

$$\theta = \frac{f}{hf_c} (\pi/2 - j\beta c/4). \quad (3)$$

Three plots of the magnitude response, $|H_h(f)|$, are given in Fig. 2. In these plots the abscissa is the normalized frequency parameter f/f_c , and the values for h are 2, 6, 10.

This model gives results that approximate frequency response measurements made using single-layer PVDF spotpoled membrane hydrophones having submillimeter active diameters [4], [6]. Bilaminar membrane hydrophones behave similarly, but the resonance peak can be accentuated [7], possibly by the presence of an additional frequency-dependent term giving rise to a linear increase in sensitivity with frequency. Because of differences in design and construction, needle-like PVDF hydrophones can display either resonant or damped behavior, and are thus more difficult to model [4], [8], [9].

C. Amplifier Response Model

A single-pole, low-pass filter was used to simulate the hydrophone amplifier response, $H_a(f)$:

$$H_a(f) = [1 + j(f/f_a)]^{-1} \quad (4)$$

where f_a is the low-pass corner frequency.

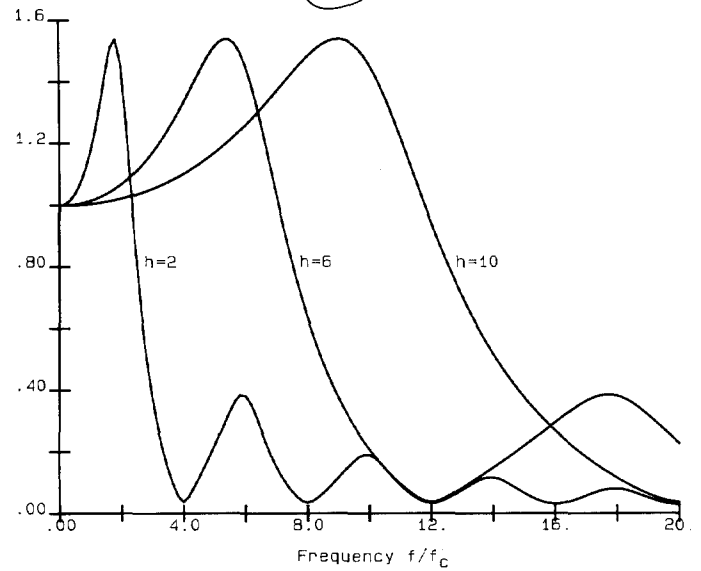


Fig. 2. Magnitude of hydrophone response function $|H_h(f)|$ versus frequency parameter f/f_c for $f_h/f_c = 2, 6$, and 10 .

As with the hydrophone model, a scaling frequency term $a = f_a/f_c$ was used to characterize the amplifier response, giving

$$H_a(f) = [1 + j(f/af_c)]^{-1}. \quad (5)$$

For stability reasons, the single-pole rolloff characteristic of (5) is a desired feature in the open-loop response of operational amplifier-based circuits, and it is typical in the greatest percentage of integrated circuit (IC) operational amplifiers [10]. Although a uniform single-pole rolloff rate is difficult to maintain in high frequency amplifiers due to the presence of parasitic elements in the circuitry, external passive compensation networks can be used to shape the open-loop frequency response to some extent (see, e.g., [11, ch. 2, p. 157]). Also, high speed IC buffer amplifiers that have been used in hydrophone amplifier circuits display single-pole characteristics over significant portions of the total response [11, ch. 3, p. 11], [12].

D. Overall Response

Fig. 3 contains a block diagram of the overall response model. The filtered pulse $p_o(t)$ is the inverse Fourier transform of the product of the hydrophone and amplifier response and the Fourier transform of (1), $P_i(f)$; i.e.,

$$p_o(t) = F^{-1}[P_i(f) \cdot H_h(f) \cdot H_a(f)]. \quad (6)$$

III. SIMULATION RESULTS

A. Amplifier Response

Equation (6) first was evaluated with $H_h(f) = 1$ (i.e., equivalent to a flat hydrophone response). The frequency term f_a/f_c was varied in steps of one from one to ten. At each frequency the values for p_c , p_r , $p^2 I$, and I_{pA} were calculated for $p_o(t)$, and the percent deviations from the corresponding $p_i(t)$ values were tabulated.

Table I contains the results for $f_a/f_c = 2, 4, 6, 8$, and

TABLE I
PERCENT DEVIATION OF PULSE QUANTITIES FOR VARIOUS AMPLIFIER
BANDWIDTHS AND $H_h(f) = 1$

	f_a/f_c				
	2	4	6	8	10
p_c	-43.0	-22.8	-13.9	-9.0	-6.8
p_r	-5.0	-1.0	-0.2	0.0	0.1
p^2I	-34.5	-14.6	-7.9	-4.9	-4.0
I_{PA}	-34.5	-14.6	-7.9	-4.9	-3.4

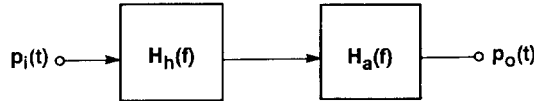


Fig. 3. Block diagram of pulse response model.

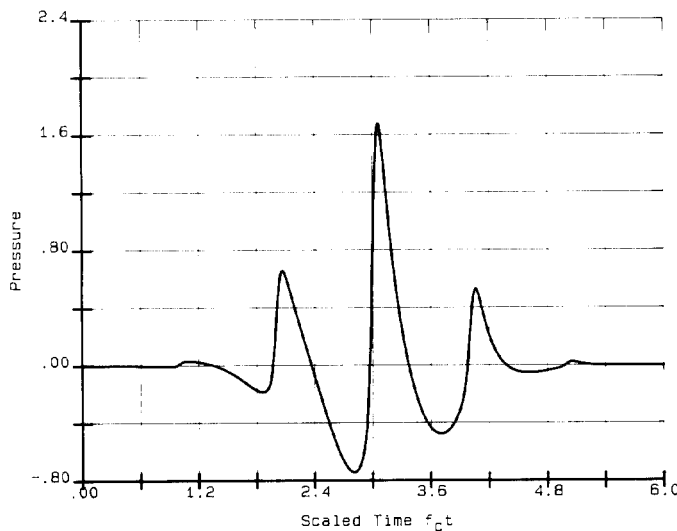


Fig. 4. Plot of $p_o(t)$ for $H_h(f) = 1$ and $f_a/f_c = 4$.

10. As can be seen from row 1 of the table, the most frequency-sensitive of the four quantities is p_c , followed closely by I_{PA} and p^2I . This is not surprising, because of the large bandwidth associated with these parameters, especially p_c . On the other hand, the negative half-cycles, and thus p_r , are relatively unaffected by changes in measurement bandwidth.

Fig. 4 contains a plot of $p_o(t)$ for $H_h(f) = 1$ and $f_a/f_c = 4$, to illustrate the decrease in p_c for $p_o(t)$ as compared to the change in p_r (cf. Fig. 1). Note from Table I that for the errors in p^2I and I_{PA} to be less than $\pm 5\%$, f_a/f_c must be greater than about 8.

B. Hydrophone Response

Setting $H_a(f) = 1$ in (6), equivalent to an ideally flat amplifier response, permits evaluation of $H_h(f)$. Similar to the above analysis, the frequency term f_h/f_c was varied from one to ten and the four pulse quantities were calculated. Percent deviations are contained in Table II for $f_h/f_c = 2, 4, 6, 8$, and 10.

The error in p_c increases (that is, becomes more posi-

TABLE II
PERCENT DEVIATION OF PULSE QUANTITIES FOR VARIOUS HYDROPHONE
BANDWIDTHS AND $H_a(f) = 1$

	f_h/f_c				
	2	4	6	8	10
p_c	-10.6	11.8	16.2	15.2	11.2
p_r	7.2	2.6	1.2	0.7	0.4
p^2I	34.3	21.2	12.6	7.7	4.8
I_{PA}	63.5	17.4	13.6	7.7	4.8

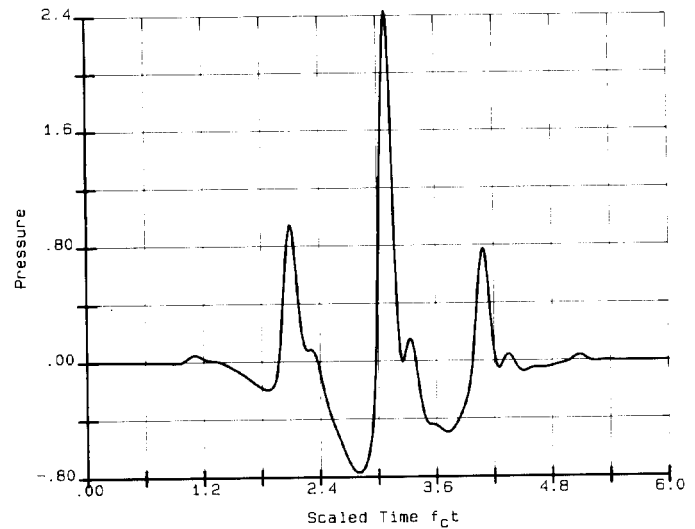


Fig. 5. Plot of $p_o(t)$ for $H_a(f) = 1$ and $f_h/f_c = 4$.

tive) before decreasing, reaching a peak at $f_h/f_c \approx 6$. This is because at low f_h/f_c values, the higher harmonics in $P_i(f)$ that give rise to the peaked positive pressure half-cycles in $p_i(t)$ are suppressed, and the error in p_c is negative. However, as f_h/f_c increases, the frequencies in $P_i(f)$ associated with these positive half-cycles become amplified by the hydrophone's thickness resonance peak. Overshoot in the positive portions of $p_i(t)$ results, and the p_c error reaches a maximum positive value before eventually decreasing as f_h becomes much greater than f_c .

The errors in p^2I and I_{PA} are positive and quite large for low f_h/f_c values, so the loss of the higher frequencies is more than compensated by the hydrophone's resonant peak. Thus, it is incorrect to assume uncritically that a limited measurement bandwidth always results in an underestimate of a pulse quantity value. Note from Table II that for the errors in p^2I and I_{PA} to be less than $\pm 5\%$, f_h/f_c must be greater than about 10.

A plot of $p_o(t)$ for $H_a(f) = 1$ and $f_h/f_c = 4$ is given in Fig. 5 (cf. Fig. 1). The perturbations on the falling portions of the positive half-cycles are similar to the hydrophone resonance-related oscillations and inflection points that have been observed in actual measurements [4, 13]. The frequency of these oscillations is approximately f_h (see Section II-B), which corresponds to a scaled time oscillation period in Fig. 5 of $f_c t = 1/h$.

TABLE III
PERCENT DEVIATION FOR p_c

f_h/f_c	f_a/f_c				
	2	4	6	8	10
2	-28.1	-16.4	-13.4	-12.2	-11.7
4	-26.6	-4.7	2.9	6.3	7.8
6	-32.6	-7.2	2.5	7.8	10.2
8	-37.9	-12.1	-1.0	4.2	7.2
10	-41.1	-16.1	-5.5	0.6	3.5

TABLE IV
PERCENT DEVIATION FOR p_r

f_h/f_c	f_a/f_c				
	2	4	6	8	10
2	-0.7	3.0	3.8	4.0	4.4
4	-2.7	1.5	2.3	2.6	2.7
6	-3.9	0.2	0.9	1.2	1.2
8	-4.4	-0.3	0.5	0.7	0.8
10	-4.6	-0.5	0.2	0.5	0.6

TABLE V
PERCENT DEVIATION FOR $p^2 I$

f_h/f_c	f_a/f_c				
	2	4	6	8	10
2	-6.2	19.9	27.2	30.1	31.5
4	-24.1	1.8	10.8	14.9	16.9
6	-29.9	-6.5	1.9	5.9	8.0
8	-32.1	-10.2	-2.4	1.2	3.2
10	-33.1	-11.9	-4.6	-1.2	0.7

TABLE VI
PERCENT DEVIATION FOR I_{PA}

f_h/f_c	f_a/f_c				
	2	4	6	8	10
2	3.9	43.2	53.4	58.4	60.2
4	-24.8	-0.6	7.3	11.2	13.3
6	-29.9	-6.5	1.9	5.9	8.0
8	-32.1	-10.2	-3.2	1.2	2.4
10	-33.1	-11.9	-4.6	-1.2	0.7

C. Combined Response

The effects of the cascaded response functions were examined by varying both f_a/f_c and f_h/f_c from one to ten in steps of one, and computing the errors as above for the 100 resultant $p_o(t)$ waveforms. Representative results are tabulated in Tables III–VI, and the data also are presented in Fig. 6 as four “error surfaces,” one each for p_c , p_r , $p^2 I$, and I_{PA} . The independent variables are f_a/f_c from front ($f_a/f_c = 1$) to back ($f_a/f_c = 10$), and f_h/f_c from left ($f_h/f_c = 1$) to right ($f_h/f_c = 10$). The error is graphed vertically.

Two general observations may be made from these results. First, as f_a/f_c increases for a given f_h/f_c , the $p_o(t)$

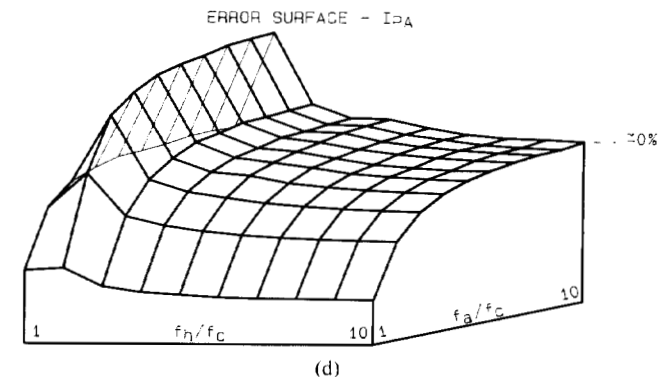
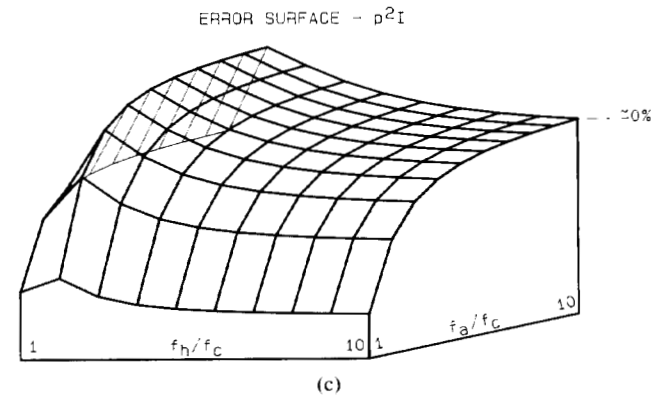
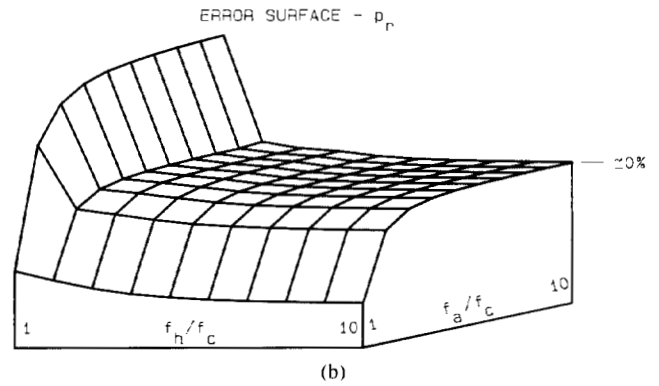
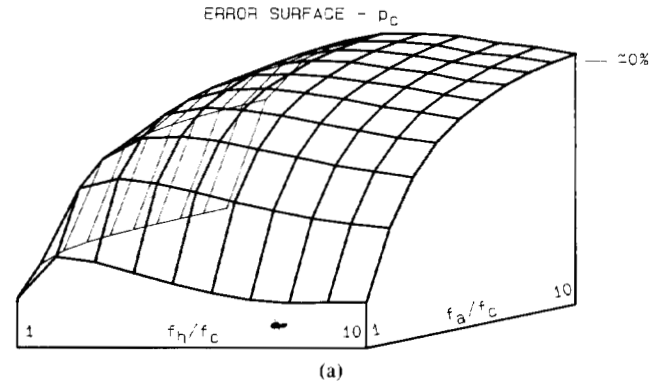


Fig. 6. Plots of “error surfaces” for (a) p_c , (b) p_r , (c) $p^2 I$, and (d) I_{PA} . See Section III-C for explanation.

pulse values also increase. Second, as f_h/f_c increase beyond 3 for a given f_a/f_c , the $p_o(t)$ pulse values decrease. Below $f_h/f_c = 3$ the behavior is erratic and less predictable.

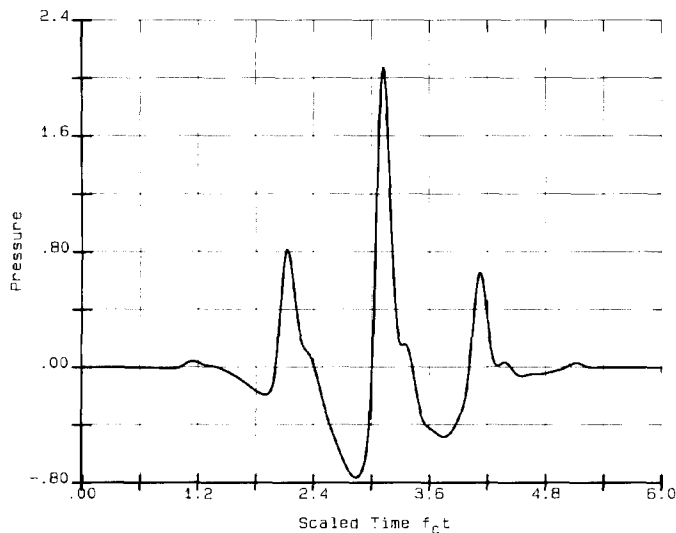


Fig. 7. Plot of $p_o(t)$ for $f_h/f_c = f_a/f_c = 4$.

These observations say nothing about the absolute error; they just point out trends in the values of the pulse quantities. However, it may be noted that because of the offsetting nature of the two response functions, the amplifier response may be tailored to minimize errors, once a hydrophone resonance frequency is known. In most cases, an optimum design would be achieved by choosing f_a to be equal to or slightly less than f_h . For example, with $f_h/f_c = f_a/f_c = 4$, all errors were less than $\pm 5\%$. Fig. 7 contains a plot of $p_o(t)$ for this situation.

IV. CONCLUSION

Because of the variety of pulses, hydrophones, and amplifiers likely to be encountered in practice, the above analysis only approximates an actual measurement situation. For example, the distorted pulse in Fig. 1 is characteristic of large amplitude pulses, and as such represents a near worst-case situation. Lower amplitude pulses lack the fast leading edges contained in Fig. 1, and for such pulses the errors will be smaller than those given here, especially for p_c . Also, as discussed in Section II-B, the hydrophone response model of (2) best fits PVDF membrane hydrophones, particularly those of the single-layer design. Furthermore, the analysis in this paper assumes that the amplifier is located close enough to the hydrophone so that transmission-line resonance effects in the connecting cable can be ignored. If this is not the case, then significant high frequency ringing can occur in pulses distorted by finite amplitude effects, with concomitant errors in pulse measurements, especially p_c [4], [13].

These potential limitations notwithstanding, however, it is believed that following the guidelines below when choosing hydrophone and amplifier bandwidths will help minimize the errors introduced by non-ideal frequency responses.

- 1) Choose the bandwidths of both the hydrophone and amplifier to be greater than 8 times that of the center frequency.

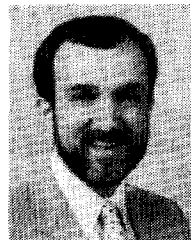
- 2) If 1) is not possible, choose the amplifier bandwidth to be equal to or slightly less than that of the hydrophone (e.g., $f_a = 0.8 - 1.0 f_h$).
- 3) If possible, avoid values of f_h/f_c or f_a/f_c below 3.

It may be noted that 1) is essentially the International Electrotechnical Commission recommendation for hydrophone bandwidth [2].

Lastly, although not the subject of this paper, it should be mentioned that spatial averaging due to the finite effective size of the hydrophone is another potentially significant source of measurement error [4], [14]. This effect should be considered along with frequency response when evaluating the overall accuracy of miniature ultrasonic hydrophones.

REFERENCES

- [1] "Safety standard for diagnostic ultrasound equipment," *AIUM/NEMA Standards Publ. ULI-1981* (in *J. Ultrasound Med. Suppl.*, vol. 2, pp. S1-S50, 1983).
- [2] "Measurement and characterization of ultrasonic fields using hydrophones in the frequency range 0.5 MHz and 15 MHz," to be published as an IEC Standard, IEC Central Office document 87(CO)6, 1988. International Electrotechnical Commission, Geneva, Switzerland.
- [3] E. J. Ayme and E. L. Carstensen, "Cavitation induced by asymmetric distorted pulses of ultrasound: Theoretical predictions," *IEEE Trans. Ultrason. Ferroelec. Freq. Contr.*, vol. 36, pp. 32-40, Jan. 1989.
- [4] G. R. Harris, "Hydrophone measurements in diagnostic ultrasound fields," *IEEE Trans. Ultrason. Ferroelec. Freq. Contr.*, vol. 35, pp. 87-101, Mar. 1988.
- [5] W. P. Mason, *Electromechanical Transducers and Wave Filters*, Princeton, NJ: Van Nostrand, 1948, second ed., pp. 200 and 399.
- [6] D. R. Bacon, "Characteristics of a pvdf membrane hydrophone for use in the range 1-100 MHz," *IEEE Trans. Sonics Ultrason.*, vol. 29, pp. 18-25, Jan. 1982.
- [7] R. C. Preston, "The NPL ultrasound beam calibrator," *IEEE Trans. Ultrason. Ferroelec. Freq. Contr.*, vol. 35, pp. 122-139, Mar. 1988.
- [8] P. A. Lewin, "Miniature piezoelectric polymer ultrasonic hydrophone probes," *Ultrason.*, vol. 19, pp. 213-216, 1981.
- [9] M. Platte, "A polyvinylidene fluoride needle hydrophone for ultrasonic applications," *Ultrason.*, vol. 23, pp. 113-118, 1985.
- [10] W. G. Jung, *IC Op-Amp Cookbook*, third ed., Howard W. Sams, Carmel, IN, 1986, pp. 49-53.
- [11] *Linear Databook 1*, Rev. 1 Nat. Semiconductor Corp., Santa Clara, CA, 1988.
- [12] Elantec EL2004/EL2004C FET Buffer Data Sheet, Rev. B. Elantec, Inc. Milpitas, CA, March 1985.
- [13] R. A. Smith, "The importance of the frequency response of a hydrophone when characterising medical ultrasound fields," *Proc. Inst. Acoust.*, vol. 8, pt 2, pp. 119-128, 1986.
- [14] R. A. Smith, "Are hydrophones of diameter 0.5 mm small enough to characterise diagnostic ultrasound equipment?," *Phys. Med. Biol.*, vol. 34, no. 11, pp. 1593-1607, 1989.



Gerald R. Harris was born in Jacksonville, NC, on November 22, 1945. He received the B.E.E. degree from the Georgia Institute of Technology, Atlanta, in 1967, the M.S. degree in biological engineering from the Rose-Hulman Institute of Technology, Terre Haute, IN, in 1971, and the Ph.D. degree in electrical engineering from the Catholic University of America, Washington, DC, in 1982.

Since 1967 he has been employed by the U.S. Public Health Service, and he is currently with F.D.A.'s Center for Devices and Radiological Health, where his main activities comprise the theoretical and experimental evaluation of medical ultrasound transducers and systems.

Dr. Harris is a member of the Acoustical Society of America, the American Institute of Ultrasound in Medicine, and Sigma Xi.